H Atom Yields from the Reactions of CN Radicals with C_2H_2, C_2H_4, C_3H_6, *trans*-2-C_4H_8, and *iso*-C_4H_8[†]

Kelly L. Gannon, David R. Glowacki, Mark A. Blitz, Kevin J. Hughes, Michael J. Pilling, and Paul W. Seakins*

School of Chemistry, University of Leeds, Woodhouse Lane, Leeds, LS2 9JT, United Kingdom

Received: December 27, 2006; In Final Form: April 13, 2007

The kinetics and H atom channel yield at both 298 and 195 K have been determined for reactions of CN radicals with C_2H_2 (1.00 ± 0.21, 0.97 ± 0.20), C_2H_4 (0.96 ± 0.032, 1.04 ± 0.042), C_3H_6 (pressure dependent), *iso*-C_4H_8 (pressure dependent), and *trans*-2-C_4H_8 (0.039 ± 0.019, 0.029 ± 0.047) where the first figure in each bracket is the H atom yield at 298 K and the second is that at 195 K. The kinetics of all reactions were studied by monitoring both CN decay and H atom growth by laser-induced fluorescence at 357.7 and 121.6 nm, respectively. The results are in good agreement with previous studies where available. The rate coefficients for the reaction of CN with *trans*-2-butene and *iso*-butene have been measured at 298 and 195 K for the first time, and the rate coefficients are as follows: $k_{298K} = (2.93 \pm 0.23) \times 10^{-10}$ cm^3 molecule^{-1} s^{-1}, $k_{195K} = (3.58 \pm 0.43) \times 10^{-10}$ cm^3 molecule^{-1} s^{-1} and $k_{298K} = (3.17 \pm 0.10) \times 10^{-10}$ cm^3 molecule^{-1} s^{-1}, $k_{195K} = (4.32 \pm 0.35) \times 10^{-10}$ cm^3 molecule^{-1} s^{-1}, respectively, where the errors represent a combination of statistical uncertainty (2σ) and an estimate of possible systematic errors. A potential energy surface for the CN + C_3H_6 reaction has been constructed using G3X//UB3LYP electronic structure calculations identifying a number of reaction channels leading to either H, CH_3, or HCN elimination following the formation of initial addition complexes. Results from the potential energy surface calculations have been used to run master equation calculations with the ratio of primary:secondary addition, the average amount of downward energy transferred in a collision $\langle \Delta E_d \rangle$, and the difference in barrier heights between H atom elimination and an H atom 1, 2 migration as variable parameters. Excellent agreement is obtained with the experimental 298 K H atom yields with the following parameter values: secondary addition complex formation equal to 80%, $\langle \Delta E_d \rangle = 145$ cm^{-1}, and the barrier height for H atom elimination set 5 kJ mol^{-1} lower than the barrier for migration. Finally, very low temperature master equation simulations using the best fit parameters have been carried out in an increased precision environment utilizing quad−double and double−double arithmetic to predict H and CH_3 yields for the CN + C_3H_6 reaction at temperatures and pressures relevant to Titan. The H and CH_3 yields predicted by the master equation have been parametrized in a simple equation for use in modeling.

1. Introduction

The atmospheres of the planets Saturn, Jupiter, Uranus, and Neptune, together with their satellites, particularly Titan, have been investigated by both space missions and experimental ground-based studies.[2−4] An interest in Titan, the largest moon of Saturn, lies in the possible similarities of its atmospheric composition to that of the early Earth atmosphere.[5,6] Titan has gained special attention as it has been found to have trace amounts of many nitrile compounds, which are thought to be key intermediates in the formation of biologically relevant molecules.[7] Unlike Earth, the temperature on Titan's surface is around 94 K, preventing the existence of liquid water and so "freezing" chemical evolution.[8] Recently, the Cassini orbiter observed the upper atmosphere of Titan for over a year before, in January 2005, the Huygens probe descended through Titan's atmosphere, rotating through 360°, imaging the cloud layers and measuring the size and abundance of haze particles and atmospheric composition via gas chromatography−mass spectrometry. With a predominantly nitrogen (∼90−99%) and methane (∼1.7−4.4% with increasing concentration in the troposphere)[9]-based atmosphere,[10] it has been proposed that the following primary processes lead to the formation of CN radicals and alkenes:

$$N_2 + h\nu\ (\lambda < 80\ \text{nm}) \rightarrow N + N(^2D)$$

$$CH_4 + h\nu \rightarrow CH_3 + H$$

$$\rightarrow {}^1CH_2 + H_2$$

$$\rightarrow {}^{1,3}CH_2 + 2H$$

$$N + CH_2 \rightarrow HCN + H$$

$$HCN + h\nu \rightarrow H + CN$$

$$CH_2 + CH_3 \rightarrow C_2H_4 + H$$

The formation of the very stable CN bond represents a net sink of atmospheric nitrogen, with the ultimate sink of the nitrile compounds being condensation at the moon's surface.

[†] Part of the special issue "M. C. Lin Festschrift".

* To whom correspondence should be addressed. Fax: +44-113-3436565. E-mail: p.w.seakins@chem.leeds.ac.uk.

10.1021/jp0689520 CCC: $37.00
Published on Web 05/31/2007

The reaction of unsaturated hydrocarbons with CN continues to be studied with reference to the production of nitrile species in the atmosphere of Titan, for example,

$$CN + C_2H_2 \rightarrow HC_3N + H$$

The unsaturated hydrocarbon multiple bond is retained in the nitrile compound product, allowing continuing photochemistry to produce a range of more complex species, precursors of species necessary for life, or components of the aerosol haze. To further our understanding of the processes occurring and to model the observations of the Cassini−Huygens mission, detailed kinetic data and yields to product channels are required. In this work, the H atom production of CN reactions with C_2H_2, C_2H_4, C_3H_6, *iso*-C_4H_8, and *trans*-2-C_4H_8 has been studied, with the possible reaction channels shown by the generic scheme below.

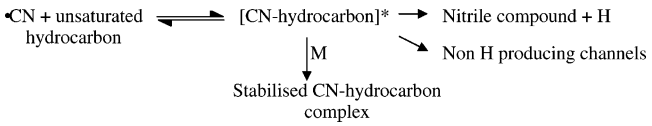

Earlier work in this laboratory[11] indicated that at room temperature the reaction of CN with C_2H_2 and C_2H_4 gives 100% H atom production. However, with the larger alkenes, the potential for direct abstraction (to form HCN and a resonantly stabilized allylic radical), non-H-producing channels (e.g., methyl elimination), or collisional stabilization increases.

Following a brief description in section 2 of the experimental methodology, section 3 outlines the use of LIF from H atoms to determine the H atom channel yields for reactions of CN with selected unsaturated hydrocarbons. Section 4 presents the results of both the kinetic and the H atom channel yield study. The pressure-dependent H atom channels discovered for both CN + C_3H_6 and CN + *iso*-C_4H_8 are investigated in section 5, where a potential energy surface (PES) for the CN + C_3H_6 system together with master equation calculations illustrate the nature of the observed H atom yield pressure dependence. The reaction of CN with CH_4 was also studied to confirm the absence of a significant H atom channel and hence also that of its coproduct CH_3CN, acetonitrile. The CH_3CN channel has been included in some photochemical models as the main source of CH_3CN production in the atmosphere of Titan[12] and has been reported as the product in some experimental studies of CN + CH_4.[7,13,14]

2. Experimental Section

All experiments were carried out in a slow-flow, stainless steel, six way cross, laser flash photolysis, laser-induced fluorescence system.[11] Gases, ICN (Fluka, ∼0.05% mix in He, BOC CP grade, 99.999%), the various hydrocarbons, C_2H_2 (Air Products Ltd., 99.9%), CH_4 (BOC gases, 99%), C_2H_4 (Aldrich, 99%), C_3H_6 (Air Products Ltd., 99%), *trans*-2-C_4H_8 (Air Products Ltd., 99%), and *iso*-C_4H_8 (Air Products Ltd., 99%), were all further purified by freeze pump thaw cycles in liquid nitrogen before being diluted and stored as ∼2.5% in He (BOC, CP grade) bath gas in glass bulbs. The diluted reagent and ICN were flowed through calibrated mass flow controllers and, via a mixing manifold, into the cell. The experiments were conducted at 298 and 195 K, with low temperatures achieved by surrounding the cell in a slurry of solid CO_2 and propan-2-ol (Fluka). Temperatures were measured just above and below the observation region with a thermocouple. While conducting these low temperature experiments, the windows of the cell were connected to a heating element, which warmed the windows, thereby preventing condensation and consequent attenuation of the signal.

The total pressure in the cell was controlled with a needle valve between the cell and the vacuum pump and measured using a Baratron pressure gauge (MKS, 0−1000 Torr). In the kinetics experiments, the flow rates of ICN and helium were held constant while the concentration of the hydrocarbon species was varied typically by a factor of 10 for total pressures of 10−200 Torr. Total gas flow rates were of the order of 5 SLM at ∼100 Torr, sufficient to ensure the complete replenishment of gas in the reaction zone between photolysis pulses.

CN radicals were generated from the unfocussed 248 nm photolysis (Lambda Physik LPX 100, ∼180 mJ/pulse, beam area ∼ 1 cm^2, and 5 Hz) of ICN.[11] Photolysis of ICN at this wavelength was determined by analysis of the resulting spectrum using the LIFBASE program,[15] to generate CN predominantly in the lowest vibrational level ($v = 0$). CN radical decay was monitored via laser-induced fluorescence pumping the B−X electronic state, (1,0) vibrational transition P_8 rotational line at 357.7 nm using an excimer-pumped dye laser (Questek vβ2000/Lambda Physik FL3002 with DMQ dye) and observing the fluorescence at $\lambda \geq 385$ nm using a Perspex filter. The delay between the photolysis and the probe pulse was varied randomly and included negative delays to give a pretrigger baseline. The reaction cell optics had one baffled vertical axis with the photomultiplier tube (PMT, Thorn EMI model 9414A) mounted directly above the reaction zone and at right angles to the excitation laser to minimize the amount of scattered laser light that the photomultiplier tube detected, ensuring that the signal observed was predominantly due to the CN LIF signal. Output from the PMT was collected via a boxcar integrator, digitized, and stored for subsequent analysis on a PC.

H atoms were monitored by vacuum ultraviolet (VUV) LIF using the Lyman-α transition (121.6 nm), achieved in this study by frequency tripling 364.110 nm radiation produced by the same tunable excimer-pumped dye laser system, in a krypton and argon mixture (Kr:Ar = 1:2.5).[16,17] The 364.110 nm light was focused by a lens (focal length = 300 mm) into a glass cell attached directly to the reaction cell. The glass tripling cell optimally contained ∼800 Torr of the Kr:Ar mixture, depending on the exact ratios of the Kr/Ar when the mix was prepared. The Lyman-α radiation generated was then coupled into the cell through an MgF_2 window. The relative VUV pulse to pulse energy output was monitored by a solar blind PMT (Thorn EMI) mounted at the window directly opposite where the tripled light entered the cell, and the probe light was reflected using a quartz flat at 45° through a VUV interference filter (Acton Research) cutting out pick-up of UV light. The H atom fluorescence was detected perpendicularly to both laser axes by a second solar blind PMT (Electron Tube). N_2(g) was flowed in front of the solar blind PMT to create an inert nitrogen atmosphere when carrying out all H atom detection experiments as any oxygen present in front of the PMT would absorb the H LIF signal.

3. Methodology

Although a highly sensitive technique, LIF does not yield absolute concentrations. Absolute calibration of the LIF signal is problematic for radical species; therefore, we use a calibration reaction to determine H atom product yields. The H atom channel yields (α) were determined by comparison of the maximum H atom signal generated from the test reaction (I_{test}) with the corresponding signal obtained under exactly the same experimental photolysis conditions from the calibration reaction

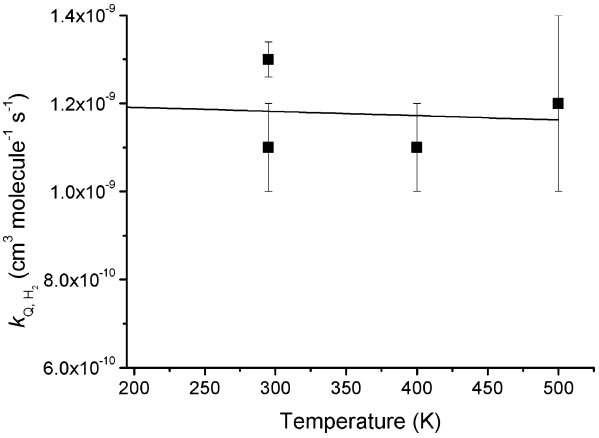

Figure 1. Plot showing k_{q,H_2} values over the temperature range 300−500 K with extrapolation to 195 K.

(I_{ref}) after making any necessary allowances for quenching or absorption of Lyman-α radiation by the substrate gases (concentrations C_{test}, C_{ref}).

$$\alpha = \frac{I_{test} \cdot C_{test}}{I_{ref} \cdot C_{ref}} \qquad \text{(E1)}$$

In this study, the technique employed by Choi et al.[11] was used to determine the H atom channel yields at both 298 and 195 K. Initially, the reaction of CN radicals with hydrogen[11] was used as the calibration reaction. This reaction is well-characterized, leading to only the production of HCN + H.[18−20]

$$CN + H_2 \rightarrow HCN + H \qquad \text{(R1)}$$

When determining the value for the H atom channel yield, α, using reaction R1 as the 100% H atom reference, a quenching factor needs to be considered to allow for the quenching of the H atom LIF signal by H_2 and its attenuation by absorption of Lyman-α radiation by H_2. The quenching coefficients and fluorescence lifetime of H (2^2P) have been determined ($k_{qH_2 295K} = 1.30 \pm 0.04 \times 10^{-9}$ cm^3 molecule^{-1} s^{-1} [11] and $k_{qH_2 195K} = 1.19 \pm 0.26 \times 10^{-9}$ cm^3 molecule^{-1} s^{-1}). The 195 K value was obtained from previous experimentally determined values[21] as shown in Figure 1, using $\tau_f = 1.6 \times 10^{-9}$ s.[21]

The quenching coefficient for H_2 (k_{q,H_2}) and the fluorescence lifetime (τ_f) were applied to the observed fluorescence signal ($I_{f,obs}$) using the following equation:

$$I_{f,corrected} = \left\{1 + \frac{k_{q,H_2}}{(1/\tau_f)} \times [H_2]\right\} \times I_{f,obs} \qquad \text{(E2)}$$

Quenching by H_2 limits the range of conditions that can be accurately studied. By confirming that the H atom production from reactions of CN with both C_2H_2 and C_2H_4 was unity (in agreement with previous studies),[11] over a wide range of pressures, at both 298 and 195 K, it was then possible to utilize these reactions as calibration systems, facilitating studies of reactions with low H atom yields. The absorption of the Lyman-α probe light by substrate was addressed in these experiments by real-time monitoring and subsequent normalization of any variation in the Lyman-α signal. The addition of a second PMT to the cell, which was able to monitor the VUV pulse to pulse energy, together with the LabVIEW program, allowed each signal point to be normalized relative to the VUV power.

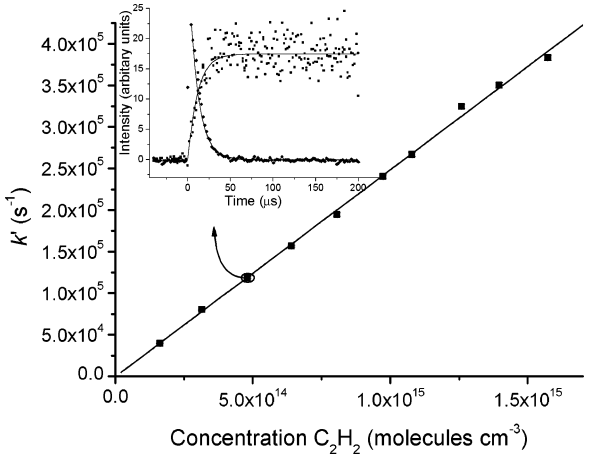

Figure 2. k' vs $[C_2H_2]$ at total pressure = 20 Torr and 298 K. The solid line represents the linear fit to extract the bimolecular rate coefficient. In the inset are typical time profiles of CN and H in the reaction of CN + C_2H_2 at 60 Torr, total pressure, and 298 K where ♦ = CN fluorescence and ■ = H atom fluorescence. The solid line in the CN decay curve is a nonlinear least-squares fit, which in the H atom growth curve represents the biexponential fit, yielding k'. The error bars on the bimolecular plot represent the statistical uncertainties (2σ) in the experimental data.

4. Experimental Results and Discussion

4.1. Kinetics. All of the data were recorded by the LabVIEW (version 6.1 National Instruments Ltd.) program on a PC and analyzed using Origin version 7.0 (OriginLab Corp.). The inset in Figure 2 is an example of corresponding CN decay and H atom growth traces, which were recorded under pseudo-first-order conditions where $[H_2]$, $[C_2H_2]$, $[C_2H_4]$, $[C_3H_6]$, [*iso*-C_4H_8], [*trans*-2-C_4H_8] >> $[CN]_0$, ensuring that CN removal was governed by first-order kinetics.

The decay of CN radicals was measured as a function of time, and a nonlinear least-squares fit was applied to the data using the following expression:

$$I_{f,CN(t)} = I_{f,CN(0)} e^{-k't} \qquad \text{(E3)}$$

where k' is the pseudo first-order rate constant for CN removal. The corresponding bimolecular rate coefficient was obtained from a plot of k' vs [reagent] as shown in Figure 2. The *y*-axis intercept values, corresponding to CN decay when there was no reactive species added, were typically less than 100 s^{-1}, indicating that greater than 99% of the CN reacted with the target substrate.

The raw signal obtained from the H atom growth was corrected twice to minimize error in the results. First, any residual H atom signal present when there was no hydrocarbon flowing into the cell was subtracted from the experimental H atom growth; this typically accounted for less than 5% of the total signal. Second, the signal was corrected for any temporal power dependence of the probe laser and attenuation by absorption, by monitoring the relative pulse to pulse energy. The H atom time profiles (Figure 2) are biexponential in nature with the growth in H atom fluorescence signal being determined by the bimolecular reaction and the decay by diffusional loss of H atoms from the system.

$$I_{f,H} = \alpha \frac{[CN]_0 k'}{k_{diff} - k'} (e^{-k't} - e^{-k_{diff}}) \qquad \text{(E4)}$$

The kinetics of reactions of CN + C_2H_2, C_2H_4, and C_3H_6 have previously been studied over a wide range of temperatures as

TABLE 1: Rate Constants for CN Reactions with C_2H_2, C_2H_4, and C_3H_6

			cm^3 molecule^{-1} s^{-1}		
reactant	T (K)	k (cm^3 molecule^{-1} s^{-1})	$10^{10}\,k_{298}$	$10^{10}\,k_{195}$	ref
C_2H_2	25−298	$2.72 \times 10^{-10}\,(T/298\text{ K})^{-0.52}\,e^{-167.2(\text{Jmol}^{-1})/RT}$	2.56	3.05×10^{-10}	46
	187−740	$2.47 \times 10^{-10}\,(T/298\text{ K})^{-0.55}\,e^{-41.8(\text{Jmol}^{-1})/RT}$	2.43	3.13×10^{-10}	47
	296−698	$2.91 \times 10^{-10}\,(T/298\text{ K})^{-0.53}$	2.90	3.64×10^{-10}	48
	294−706	$3.49 \times 10^{-11}\,e^{4723.4(\text{Jmol}^{-1})/RT}$	2.34	6.43×10^{-10}	49
	298	$k_{298}\,2.31 \pm 0.091 \times 10^{-10}$	2.31		50
	259−396	$4.98 \pm 1.64 \times 10^{-11}$			51
	195, 298		2.34 ± 0.12	2.50 ± 0.13	this work (monitoring CN)
	195, 298		2.27 ± 0.18	2.43 ± 0.30	this work (monitoring H)
C_2H_4	298	$k_{298}\,2.51 \pm 0.199 \times 10^{-10}$	2.51×10^{-10}		52
	25−295	$2.67 \times 10^{-10}\,(T/298\text{ K})^{-0.69}\,e^{-250.8(\text{Jmol}^{-1})/RT}$	2.41×10^{-10}	3.06×10^{-10}	46
	95−698	$2.51 \times 10^{-10}\,(T/298\text{ K})^{-0.24}$	2.51×10^{-10}	2.78×10^{-10}	48
	294−696	$4.72 \times 10^{-11}\,e^{4221.8(\pm 167.2\text{Jmol}^{-1})/RT}$	2.59×10^{-10}	6.38×10^{-10}	49
	294	$k_{294}\,2.71 \pm 0.108 \times 10^{-10}$			50
	259−396	$4.98 \pm 0.0847 \times 10^{-11}$			51
	195, 298		2.91 ± 0.18	3.66 ± 0.26	this work (monitoring CN)
	195, 298		3.21 ± 0.62	3.49 ± 0.91	this work (monitoring H)
C_3H_6	160−298	$1.73 \times 10^{-10}\,e^{836(\text{Jmol}^{-1})/RT}$	2.43×10^{-10}	2.90×10^{-10}	46
	297−673	$1.32 \times 10^{-10}\,e^{2006.4(\pm 794\text{Jmol}^{-1})/RT}$	2.97×10^{-10}	4.55×10^{-10}	53
	294−698	$3.4 \times 10^{-10}\,(T/298\text{ K})^{-0.19}$	3.40×10^{-10}	3.69×10^{-10}	48
	294	$k_{294}\,2.31 \pm 0.299 \times 10^{-10}$			50
	195, 298		3.18 ± 0.21	3.25 ± 0.20	this work (monitoring CN)
	298		2.74 ± 0.18		this work (monitoring H)
trans-2-butene	195, 298		2.93 ± 0.20	3.58 ± 0.23	this work (monitoring CN)
iso-butene	195, 298		3.17 ± 0.17	4.32 ± 0.26	this work (monitoring CN)
	298		3.30 ± 0.47		this work (monitoring H)

summarized in Table 1. These reactions are fast, with similar negative temperature dependencies, suggesting that they proceed via a common mechanism. Table 1 also shows the results from this work, which are in good agreement with the literature values. Within error, the same bimolecular rate coefficient is obtained whether monitoring CN decay or H atom production. The reaction of CN with both *trans*-2-C_4H_8 and *iso*-C_4H_8 has not been studied previously; however, the CN kinetic data are of the same order of magnitude and exhibit the same negative temperature dependence as for CN + C_2H_2, C_2H_4, and C_3H_6 as summarized in Table 1.

A major objective of this work was to investigate whether new reaction channels become available for C_3 and C_4 species. CN is a pseudo-halogen; therefore, one might expect there to be analogies with the corresponding Cl atom reactions. Pilgrim and Taatjes studied the reaction of Cl with C_3H_6 over the temperature range of 293−800 K and a pressure range of 3−10 Torr using a laser photolysis/infrared long-path absorption technique[22] and found the direct H atom abstraction channel to HCl and C_3H_5 to have a weak positive temperature dependence. This suggests that the direct H atom abstraction channel to HCN and an allylic type radical would be expected to have a positive temperature dependence. However, the observed negative temperature dependence of the CN + propene reaction shows that a channel with a positive activation energy can only be a minor contributor to the overall reaction. The similarity of the temperature dependence of all of the CN reactions suggests that they proceed via the same initial complex-forming step.

The bimolecular rate coefficients obtained by monitoring CN decay for the reactions of CN with C_2H_2, C_2H_4, and *iso*-C_4H_8 were studied as a function of pressure, to see if these reactions exhibited any form of pressure dependence due to stabilization of the unstable CN-unsaturated hydrocarbon adduct. The reaction with C_2H_2 was studied over the range of 25−400 Torr at 298 and 195 K, C_2H_4 over the range of 25−300 Torr at 298 and 195 K, and *iso*-C_4H_8 over the range of 5−100 Torr at 298 K. Figure 3 shows the results, which indicate that for these compounds under all conditions studied, there is no pressure dependence in the bimolecular rate constant.

The variance of the rate coefficients measured as a function of pressure is a more realistic assessment of the overall error in the rate coefficients rather than the regression statistics for one bimolecular plot as reported in Table 1. Typical percentage errors (2σ) from the pressure dependence measurements are of the order of 5−8%, and these are the errors reported.

The rate coefficients for the reaction of CN with methane were also measured by monitoring CN decay at 298 and 195 K. The resulting values, $k_{298} = (8.45 \pm 0.10) \times 10^{-13}$ cm^3 molecule^{-1} s^{-1} and $k_{195} = (1.44 \pm 0.05) \times 10^{-13}$ cm^3 molecule^{-1} s^{-1}, are in good agreement with recent literature determinations (e.g., $k_{300} = 8.58 \times 10^{-13}$ cm^3 molecule^{-1} s^{-1},[23] $k_{200} = 1.37 \times 10^{-13}$ cm^3 molecule^{-1} s^{-1}).[24]

4.2. H Atom Yield Studies. Table 2 summarizes the H atom channel yields obtained when studying CN reactions with C_2H_2, C_2H_4, CH_4, C_3H_6, *iso*-C_4H_8, and *trans*-2-C_4H_8 at both 298 and 195 K, where the errors represent a combination of statistical uncertainty (2σ) and an estimate of possible systematic errors. It was found that two of these reactions (C_2H_2 and C_2H_4) led to 100% H atom production, two did not exhibit any significant H atom production (CH_4 and *trans*-2-C_4H_8), and two (C_3H_6 and *iso*-C_4H_8) showed pressure-dependent H atom production.

4.2.1. CN + C_2H_2, C_2H_4. For the reaction of CN with acetylene, there is only one open channel to H atom production, but the possibility of stabilization of the addition complex formed when CN adds to the π system also exists (reaction R2).

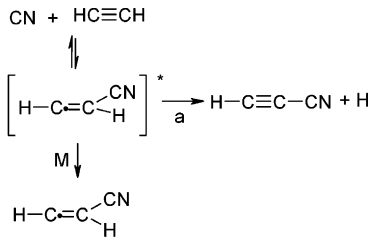

(2a) $H_r = -90$ kJ mol^{-1} [1]

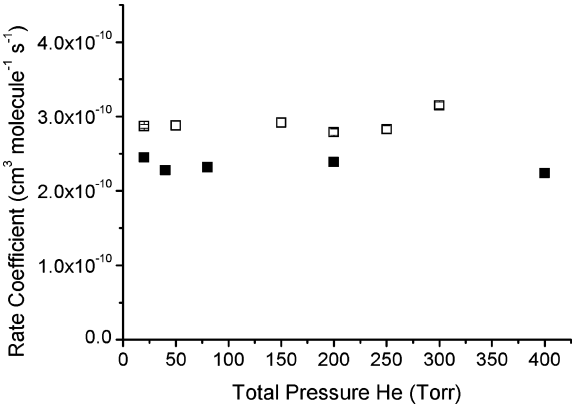

Figure 3. Pressure dependence of the bimolecular rate coefficient for the reaction of CN + selected unsaturated hydrocarbons at 298 and 195 K where ■ = CN + C_2H_2 at 298 K and □ = CN + C_2H_4 at 298 K.

TABLE 2: Summary of H Atom Yield Studies

	H atom channel yields	
reagent	298 K	195 K
C_2H_2	1.00 ± 0.21	0.97 ± 0.20
C_2H_4	0.96 ± 0.03	1.04 ± 0.04
CH_4	upper limit 0.040	upper limit 0.053
C_3H_6	pressure dependent k_{4d}/k_{4a} = 0.082 ± 0.022 cm^3 molecule^{-1}	pressure dependent k_{4d}/k_{4a} = 0.148 ± 0.067 cm^3 molecule^{-1}
trans-2-C_4H_8	0.039 ± 0.019	0.029 ± 0.047
iso-C_4H_8	pressure dependent k_{5d}/k_{5a} = 0.182 ± 0.018 cm^3 molecule^{-1}	pressure dependent k_{5d}/k_{5a} = 0.24 ± 0.25 cm^3 molecule^{-1}

For ethene, there is also the possibility that the vinyl radical and HCN could be formed. This may proceed via an addition−elimination type mechanism (as shown, reaction R3) or via a direct abstraction channel.

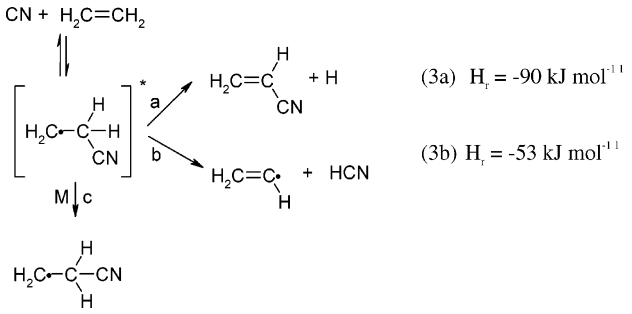

The room temperature results are in good agreement with those from the previous studies by Choi et al.[11] where the channel yield (2a) was determined to be $\alpha_{2a} = 1.08 \pm 0.13$ and that of reaction 3a was $\alpha_{3a} = 1.04 \pm 0.11$ over the pressure range of 15−55 Torr at 298 K. The results are consistent with earlier investigations by Balucani et al.,[25] where the dynamics of these reactions were studied using a crossed molecular beam apparatus with angularly resolved mass spectrometric observation of products. The only products detected were C_3HN and C_3H_3N (for reactions of CN + C_2H_2 and C_2H_4, respectively). These were rationalized to be HC_2CN and C_2H_3CN, implying coupled H atom production, which would be consistent with the 100% yield of H atom observed by Choi et al.[11] In the present study, the room temperature and low temperature fractional channel yield for H atom production for both reactions R2 and R3 have been determined as $\alpha_{2a,295K} = 1.00 \pm 0.21$, $\alpha_{2a,195K} = 0.97 \pm 0.20$, $\alpha_{3a,295K} = 0.96 \pm 0.03$, and $\alpha_{3a,195K} = 1.04 \pm 0.04$ as shown in Figure 4. The low temperature yields for these reactions have not been studied previously. Over the experimental range, 20−80 Torr and 295−295 K, there is no collisional stabilization of the unstable CN adduct, and for the C_2H_4 reaction, the channel to produce HCN + C_2H_3 is not active, with all reacting CN + C_2H_2/C_2H_4 forming H atoms.

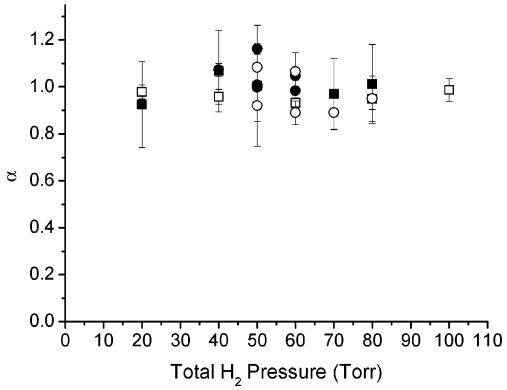

Figure 4. H atom yield as a function of total H_2 pressure at both 295 and 195 K for reactions of CN + C_2H_2 and CN + C_2H_4 where ■ = CN + C_2H_2 at 295 K, □ = C_2H_4 at 295 K, ● = C_2H_4 at 195 K, and ○ = C_2H_2 at 195 K.

Reaction R3 has been modeled by Vereecken et al.,[26] who developed the original ab initio surface used by Balucani et al. and then modeled the pressure and temperature dependence of the product yields via RRKM/master equation calculations. In agreement with the current work, they calculated that at 300 K, channel 3a will be dominant at low pressures, with the stabilization channel only becoming significant (10%) at approximately 400 Torr. At 195 K, stabilization is predicted to be significant at slightly lower pressures but still above those measured in this study.

4.2.2. CN + C_3H_6, iso-C_4H_8. For the reaction of CN with propene, there are several possible product channels as shown by the schematic associated with reaction R4. There are two possible sites for CN addition with addition at the terminal CH_2 site being more favorable, as this would generate a more stable secondary radical. From either of these two addition sites, the methyl group or H atom could be lost to regenerate the double bond, or there could be collisional stabilization of the excited addition complex (4d). There is a hydrogen atom abstraction channel or addition/elimination process to form the allyl radical and HCN. This channel is comparatively more thermodynamically favorable than the equivalent channel for reaction R3 because of the enhanced stability of the allyl radical (reaction R4).

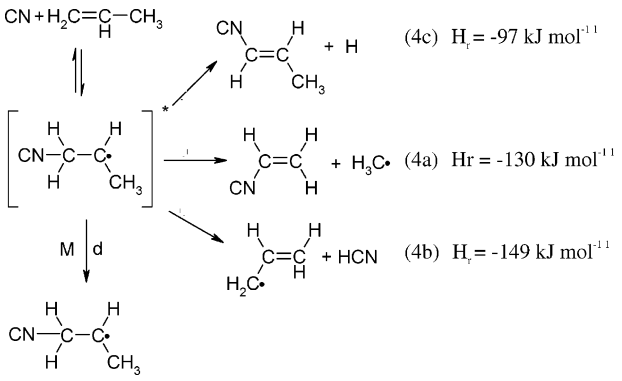

Similar reaction products to reaction R4 are available from the reaction of CN with *iso*-butene (reaction R5). In comparison

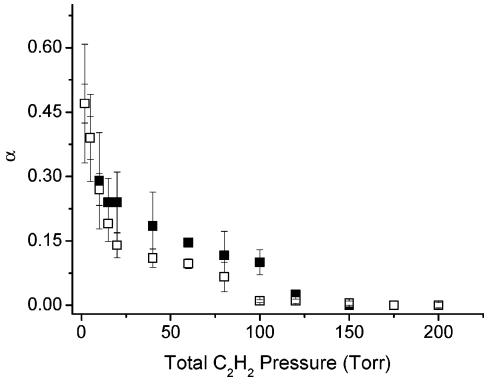

Figure 5. Pressure dependence of the H atom yields for reactions CN + C_3H_6 (■) and CN + *iso*-C_4H_8 (□) at 298 K.

TABLE 3: Pressure Dependence in H Atom Yield for Reactions of CN + C_3H_6 and CN + *iso*-C_4H_8 at 298 K

	α			
total pressure (Torr)	CN + C_3H_6	±	CN + *iso*-C_4H_8	±
2	0.478	0.045	0.473	0.139
5	0.392	0.050	0.398	0.102
10	0.277	0.037	0.291	0.112
15	0.192	0.041	0.240	0.056
20	0.141	0.028	0.242	0.070
40	0.110	0.022	0.185	0.079
60	0.097	0.011	0.101	0.030
80	0.066	0.034	0.146	0.011
100	0.017	0.004	0.116	0.056
120	0.012	0.005	0.025	0.005
150	0.005	0.005	0.008	0.005
200	0.003	0.006	0.002	0.007

to propene, addition to form the primary adduct, with the potential to eliminate methyl radicals, will be less favorable because of the decreased stability of primary radicals and steric hindrance by the methyl groups, which hinder formation of the primary radical. As will be demonstrated in the following section, H atom migration and methyl radical elimination in reaction R4 may possibly compete with direct H atom elimination, such that this possibility cannot be ruled out for reaction R5 (no thermodynamic data available).

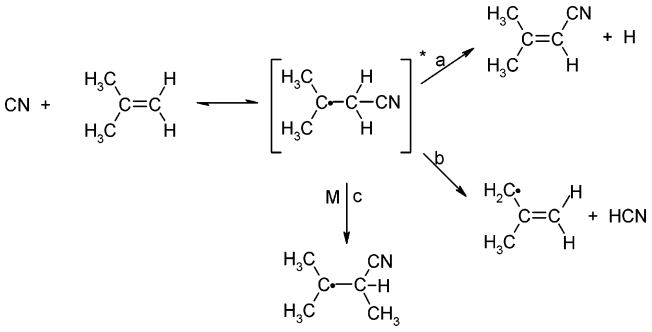

The H atom yields of CN + C_3H_6 and CN + *iso*-C_4H_8 were both studied over a He pressure range of 2−200 Torr at 298 K. As shown in Figure 5, both reactions exhibited pressure dependence for the H atom channel yield, α, with α ≈ 0.5 at low pressures, and decreasing with increasing pressure so that no H atom fluorescence was observable at ∼120 Torr (Table 3).

A linear Stern−Volmer plot was obtained by plotting α^{-1} vs total pressure as shown in Figure 6 and eq E5 for the example of CN reacting with propene, with the gradient of the straight line yielding the ratio of complex dissociation to H atoms (k_{4c}) to quenching (k_{4d}).

$$\frac{1}{\alpha} = 1 + \frac{k_{4a}}{k_{4c}} + \frac{k_{4b}}{k_{4c}} + \left(\frac{k_{4d}}{k_{4c}}\right)[\mathrm{M}] \qquad \text{(E5)}$$

The value for the intercept should be unity, if only channels 4/5c and 4/5d (H atom production and collisional stabilization of the energized CN adduct) are occurring. The observed intercept is significantly greater than unity, indicating that, even at zero pressure (and hence with no collisional stabilization), H atom elimination is not the sole reaction taking place.

The linear fit of the C_3H_6 data gives a value of 2.24 for the intercept (lower and upper 95% confidence limits of 1.23 and 3.26, respectively), indicative of other active channels at zero pressure and a ratio of $k_d/k_a + k_b + k_c$ rate coefficients of 0.082 ± 0.022 cm^3 $molecule^{-1}$. From the *iso*-C_4H_8 data, a value of 1.77 is determined for the intercept (lower and upper 95% confidence limits of 1.31 and 2.23, respectively), again characteristic of another active channel. A value of 0.182 ± 0.018 cm^3 $molecule^{-1}$ is obtained for the gradient of the Stern−Volmer plot for reaction R4 at 298 K. The gradient for reaction R5 (CN + *iso*-butene) is sensibly larger than that for propene (0.182 vs 0.082 cm^3 $molecule^{-1}$); assuming a statistical distribution of energy, dissociation of the larger CN/isobutene addition complex should be slower, giving more opportunity for stabilization to occur. The 195 K data support the 298 K data in showing pressure dependence and, as expected, an increase in the ratio of the rate constants for stabilization and H atom production, although, because of the difficulties in obtaining strong signals at low pressures and low temperatures, the results have large uncertainties.

4.2.3. CN + trans-2-C_4H_8. For the reaction of CN with *trans*-2-C_4H_8 (reaction R6) over the pressure range studied (0−100 Torr) at 298 K, the H atom production was 0.039 ± 0.019. No pressure dependence was exhibited by the reaction. At 195 K, the reaction was studied over the pressure range of 40−100 Torr, and the yield was determined to be 0.029 ± 0.047. Again, no pressure dependence and a very low yield for this reaction were observed, indicating that the reaction does not produce any H atoms within the limits of experimental error. A lack of thermodynamic data precludes comment on the relative stability of the available product channels, but the results indicate that the reaction of CN with *trans*-2-C_4H_8 + CN results in either loss of a CH_3 group instead of a H atom or HCN formation addition or abstraction. Addition to either of the identical carbon atoms on the double bond will lead to an intermediate that can either lose H or CH_3. It is most likely that the reaction will be dominated by the loss of the more stable group. Loss of HCN may also be a viable channel, as this would generate a resonance-stabilized allylic radical product.

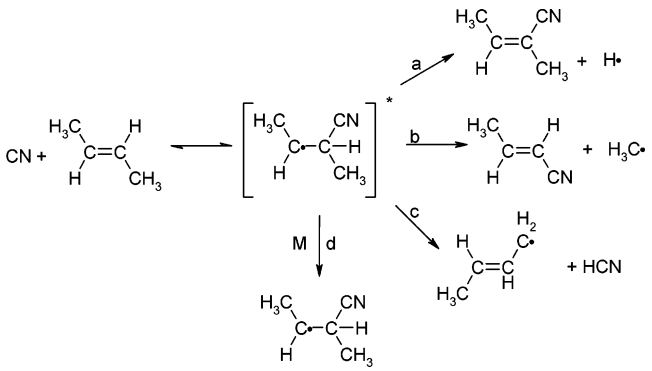

4.2.4. CN + CH₄. The H atom production for reaction R7 was investigated to clarify that this reaction does not lead to

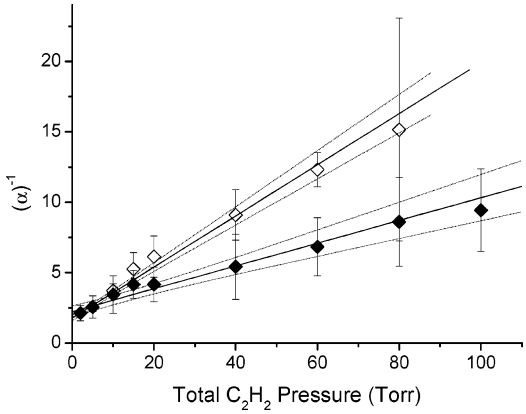

Figure 6. (H atom yield)$^{-1}$ vs total pressure yielding the quenching coefficients for the reactions of CN + C_3H_6 (♦) and *iso*-C_4H_8 (◇) at 298 K shown with 95% confidence limits.

significant formation of H atoms and acetonitrile and can therefore be disregarded as a possible channel for formation of these products in Titan atmospheric models.[6,12]

$$CH_4 + CN \rightarrow HCN + CH_3 \quad \Delta H_r = -79 \text{ kJ mol}^{-1}{}^{11} \quad \text{(R7a)}$$

$$CH_4 + CN \rightarrow CH_3CN + H \quad \Delta H_r = -68 \text{ kJ mol}^{-1}{}^{1} \quad \text{(R7b)}$$

As expected, given that channel 7b will have a significant activation barrier, there appeared to be no H atom production from reaction R7, and when analyzed, only an upper limit could be assigned to the H atom production channel of 0.04 at 298 K and 0.05 at 195 K. The experiments were repeated several times, and many of the values lie at zero with no assignable production due to the reaction. It should be noted that, as for reaction R6, in no case was it possible to observe a growth in H atom production that matched the kinetics of CN removal, and the magnitude of the upper limits may be attributed to background noise/PMT overload, which are comparable to the systematic errors (5−7%) of the experiment.

5. Theoretical Studies

5.1. PES Calculation. Electronic structure calculations and subsequent master equation simulations were undertaken to investigate the pressure dependence of the H atom yields observed in the experiments conducted on the CN + propene system and to gain some insights into the identity of the non-H atom-producing channels.

The master equation calculations require determination of the relevant minima and first-order saddle points on the PES. Geometry optimizations were performed using density functional theory (DFT) with the hybrid B3LYP functional (in its spin-unrestricted form for radicals and in its spin-restricted form for closed shell species) and the 6-311+G(3df,2p) basis set. Frequency calculations were carried out on all optimized stationary point geometries, and the eigenvalues of the calculated Hessian were examined to verify the character of the stationary point. All first-order saddle points contained exactly one imaginary eigenvalue, corresponding to the reaction coordinate. In addition to examining the displacement vector corresponding to the imaginary frequency of the Hessian, internal reaction coordinate (IRC) calculations were carried out on all first-order saddle points to verify connection with the relevant wells. B3LYP/6-311+G(3df,2p) geometry optimizations have been shown to achieve accurate geometries, zero-point energies, and frequencies as well as featuring a high computational efficiency;[27,28] however, DFT relative energies have not been shown to be sufficiently reliable for the purpose of kinetics modeling,[29]where accuracy that is within a few kJ/mol is often necessary.

The G3X method was utilized to accurately calculate the energies of the relevant stationary points for the PESs considered in this work. G3X has been shown to give accurate energies for those molecules featured in the G3/99 test set.[27] In the G3X method, electron correlation is treated by Møller Plesset perturbation theory and quadratic configuration interaction. Details of the calculations and tabulated values of rotational constants, frequencies, and energies of the intermediates and transition states can be found in the Supporting Information.

No previous PES calculations have been carried out for the CN + propene system but have been performed on similar systems.[26,30,31] The stationary points are shown in Figure 7, and the accompanying data for the DFT and G3X energies can be found in the Supporting Information. All calculations were carried out using Gaussian 03,[27] while optimized geometries and normal mode displacement vectors were viewed using GaussView 3.09.[27]

Terminal addition (one-addition) of CN forms Int1, the 1-cyanopropyl radical, while two-addition forms Inta1. Int1 reacts by: (i) isomerization (^{1,2}H shift) via TS1a to form an energized $NCCHCH_2CH_s$ radical (Int2a), which can be stabilized or can eliminate CH_3, via TS2a(i) to form the products of reaction 4a. Int2a can also eliminate H via TS2a(ii) to form 2-cyanopropene; (ii) isomerization via TS1b to form Int2b, with subsequent elimination of HCN to form the products of reaction 4b; and (iii) elimination of H via TS1c to form the products of reaction R4c.

An important feature of the surface, which is discussed in greater detailed below, is the close energy separation between TS1a and TS1c. PES calculations for similar systems involving CN adding to an unsaturated bond, such as CN + C_2H_2, CN + C_2H_4, and CN + CH_3CCH, also show similar energies for the transition states involving the [1,2] H shift and the H elimination.[26,32] Two-addition of CN to propene, to form the energized radical $CH_2CH(CN)CH_3$ (Inta1), leads directly to CH_3 elimination via TSa1 and H elimination via TSa2. TSa1 lies 25 kJ mol^{-1} below TSa2.

The master equation calculations described below did not include the direct hydrogen abstraction channel by CN from propene. By analogy with experiments performed by Pilgrim and Taatjes[22] on the direct abstraction of a propene H atom by Cl, a positive temperature dependence for the abstraction channel was observed, such that we might conclude that direct abstraction is not taking place to any significant extent in reactions R4−R6 given the relative magnitude and temperature dependence of the rate constants. However, Sreedhara et al.[33] located saddle points and geometries along the reaction coordinate for H abstraction by CN in methane, ethane, and propane at the UHF/6-31G** level. Higher level PUMP2(full)/6-31G** energy calculations were then performed on these reaction coordinate geometries, and the authors concluded that abstraction from a primary C−H bond has a small activation barrier, while abstraction from a secondary or tertiary C−H bonds has no activation barrier. This suggests that direct abstraction could be a feasible process for reactions R4−R6 where the weaker allylic C−H bond is broken.

The PES for a direct abstraction in reaction R4 from the methyl group to form HCN + allyl was therefore investigated. A first-order saddle point corresponding to abstraction of H from the methyl group in propene was located at the UHF/6-311+G-

(d,p) level of theory; however, spin contamination was significant such that the geometry was reoptimized at the ROHF/6-311+G(d,p) level. Larger basis sets were unable to locate the saddle point. Then, an IRC calculation was carried out on these reaction coordinate geometries at the UMP2/6-311+G(d,p) level. The results indicate this process to be barrierless, and the reaction rate is probably determined by dynamical constraints. The possible role and identification of a direct abstraction process are discussed below.

5.2. Master Equation Calculations. Master equation calculations were used to model the experimental H atom yields on the PES shown in Figure 7. The energy-grained master equation has been previously described.[34,35] Briefly, the population of rovibrational energy levels in different isomers on the PES is lumped into energy grains, and the population in each grain is described by a set of coupled differential equations that account for collisional energy transfer within each isomer as well as isomerization and dissociation. Microcanonical rate coefficients for the unimolecular reactions that occur in each energy grain, $k(E)$, were calculated from the PES data pertaining to the reagents and transition states via eq E6

$$k(E) = \frac{W(E)}{h\rho(E)} \tag{E6}$$

where $W(E)$ is the sum of rovibrational states at the optimized first-order saddle point geometry and $\rho(E)$ is the density of rovibrational states of the reactant. To relate the ME calculation directly to experimental rate coefficients, the microcanonical rate constants for dissociation from the initial radical adducts to regenerate the reactants were calculated using inverse Laplace transformation (ILT).[36] These rate constants were also used, by detailed balance, to calculate the energy-resolved rates of formation of the initial adducts.

Rates of collisional energy transfer were estimated using an exponential down model, expressed as

$$P(E \leftarrow E') = C(E')\exp\left(-\frac{E' - E}{\langle \Delta E_d \rangle}\right) \tag{E7}$$

where $E' > E$, $C(E')$ is a normalization constant, and $\langle \Delta E_d \rangle$ is the average energy transferred per collision in a downward direction. In this work, $\langle \Delta E_d \rangle$ was left as an adjustable parameter in a χ^2 surface-fitting routine, to be discussed later. The probability distribution for energizing collisions is related to that of downward transitions via detailed balance. The form of the master equation used in this work is

$$\frac{d|w\rangle}{dt} = \mathbf{M}|w\rangle \tag{E8}$$

where $|w\rangle$ is a vector containing the concatenated populations of the grains for each isomer and **M** is the matrix that describes collisional energy transfer, isomerization, and dissociation. The problem specification is completed by adding a final element to $|w\rangle$ to describe the CN reactant in excess propene and modifying **M** with a bimolecular source term to describe the fractional rates of population of the entrance well by the reactants. With the addition of a pseudo-first-order source term to eq E6, the master equation (E8) may be treated as an eigenvalue problem wherein **M** is diagonalized, and the eigenpair solutions are obtained. In this work, the size of the energy grains depended on the temperature, because a convergent solution requires the grain size to be smaller than $\langle \Delta E_d \rangle$, and $\langle \Delta E_d \rangle$ was found to be temperature-dependent. Having obtained the solution eigenpairs, the analysis described by Klippenstein and Miller[28] was used to calculate the rate coefficient, k_{Ri} (the phenomenological rate coefficient for the reactants forming the stabilized adduct) and k_{Rp} (the phenomenological rate coefficient for the reactants going to bimolecular products). The experimentally observed total rate of loss of reactants, k_{TR}, was obtained as the sum of the k_{Ri} and k_{Rp}. In the one well simulations, the amount of product formation vs stabilization was taken as $k_{Rp}/(k_{Ri} + k_{Rp})$. All calculations were carried out on a Beowulf cluster, which runs the RedHat Linux 2.4.21 operating system, has 20 nodes, 2 GB memory per node, and two 32-bit Intel Xeon processors per node.

Low temperature energy-grained master equation simulations are notoriously problematic for numerical reasons,[37,38] since the ratio of the smallest eigenvalue to the largest eigenvalue obtained from diagonalization of the collision matrix often exceeds machine precision. Frankcombe and Smith[38] demonstrated that carrying out master equation algorithms in a high precision environment facilitates low temperature simulations. The numerical problems that arise are particularly pronounced for systems that have a deep well, such as the system under investigation here. To address these numerical issues, we implemented the C++ double−double and quad−double arithmetic package designed by Hida et al.[39] The 298, 195, and 160 K results in this paper were carried out using double−double arithmetic, which allows for 32 digits of precision on our machine, and the 90 K results were carried out using quad−double arithmetic, which allows for 64 digits of precision on our machine. At temperatures lower than 400 K, long double precision, which is available in standard C and C++, gave unreliable results. The unreliability of these calculations was confirmed by examining (i) the time-dependent profiles of CN, any intermediates on the surface, and any products; (ii) the rate coefficients obtained from the eigenpair analysis described above; and (iii) the eigenvalue spectrum obtained from diagonalization of the collision matrix. In this system, the double−double results are essentially identical to the quad−double results down to ~140 K. Below 140 K, the double−double results diverge from the quad−double results. The quad−double results appear to give unreliable species profiles and rate coefficients below ~80 K, depending on the size of the collision matrix. For the 298 and 195 K simulations, the collision matrix was cast as 400 discrete 125 cm^{-1} grains and 500 discrete 90 cm^{-1} grains, respectively. For the 160 and 90 K simulations, it was cast as 600 discrete 70 cm^{-1} grains and 700 discrete 50 cm^{-1} grains, respectively. Changing the grain size was necessary for two reasons: (i) A convergent solution to the master equation requires that the grain size is smaller than $\langle \Delta E_d \rangle$ such that grain size must reflect the form of the $\langle \Delta E_d \rangle$ temperature dependence and (ii) the exponential down model calculates the probability of activating collisions, and the size of the collision matrix must be adjusted such that the tiny probabilities for these collisions at low temperatures and smaller values of $\langle \Delta E_d \rangle$ do not exceed the smallest value that the machine can hold (on our machine, limits are from 1.7×10^{-308} to 1.7×10^{308}) The form of the $\langle \Delta E_d \rangle$ temperature dependence is discussed below. The time required to carry out a single calculation with double−double arithmetic is a factor of 3 longer than the time required to carry out a calculation in standard C++ long double arithmetic, and a quad−double arithmetic calculation was approximately a factor of 16 slower than a long double calculation.

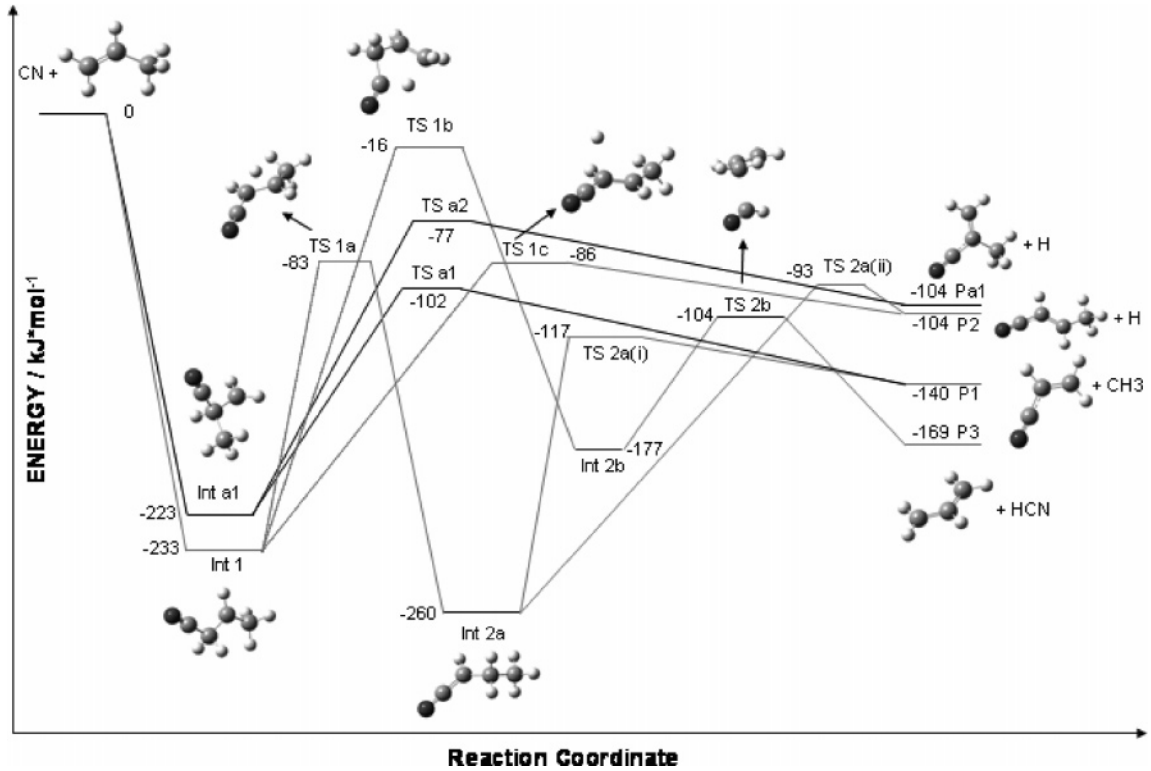

Figure 7. G3X/UB3LYP/6-311+G (3df,2p) PES for the CN + propene reaction at 0 K.

To calculate partitioning between the products obtained by the Klippenstein Miller analysis described above, the equation that describes the phenomenological rate of product formation,

$$\frac{\mathrm{d}P(t)}{\mathrm{d}t} = \sum_E k(E)\, n_E(t) \qquad \text{(E9)}$$

where $n_E(t)$ is the time-dependent population of the energy grains in the relevant well, was numerically integrated over time to give the equation

$$P(t) = \int_t \sum_E k(E)\, n_E(t)\, \mathrm{d}t \qquad \text{(E10)}$$

Using this equation, product fractions were integrated over 120 time points from 1.2×10^{-11} s to 10 s. The values of $\mathrm{d}P(t)/\mathrm{d}t$ are essentially zero at these limiting short and long times, and this time domain adequately accounts for product formation. The product fractions may be obtained using k_{Ri}, k_{Rp}, and k_{TR} eq E10, normalized to consider all available product channels. The procedure used to determine the best fit parameters for the master equation analysis is discussed below.

The process of fitting the ME parameters to the experimental data requires many implementations of the ME, and computational efficiency is essential. Accordingly, the reaction system was simplified as much as possible, and the process was then checked a posteriori, using the best fit parameters, but with a more compete reaction model. The ME analysis for fitting to the experimental data was run as two separate one well systems, including only stabilization into Int1 and Inta1. Reaction from Int1 included redissociation to CN + propene, and isomerization or dissociation via TS1a, TS1b, and TS1c were assumed to give the products specified in reactions R4a−c, respectively. Reaction from Inta1 included redissociation to CN + propene and reaction via TSa1 and TSa2 to give CH_3 and H, respectively, with the corresponding alkenes. This simplification was based on the following observations.

(i) While there are three H-producing channels from Int1 [via TS1c, TSa2, and TS2a(ii)], the only significant channel is that via TS1c. The channel via TSa2 competes unfavorably with the much lower energy TSa1 at all significant reaction energies, as shown by the microcanonical rate constants in Figure 8. Reaction from Int2a via TS2a(ii) is much slower than CH_3 elimination via TS2a(i).

(ii) With these simplifications, Int2a is either collisionally stabilized or dissociates to form CH_3 via TS2a(i). The relative importance of these channels was investigated by running a two well ME, which incorporated Int1, and Int2a with collisional relaxation in both wells, redissociation from Int1 to regenerate CN, and reaction via TS1a, TS1c, Int2a, TS2a(i), and TS2a(ii). These two well simulations, run at a range of pressures and temperatures, showed that collisional stabilization into Int2a was insignificant over the experimental pressure range (0−200 Torr). At 200 Torr and 90 K, the rate of formation of Int2a by collisional relaxation was less than 0.1% of the rate of loss of the reactants. In addition, the yields of CH_3 and H returned from the two well ME simulations were within 1% of the yields obtained from a one well simulation that does not consider stabilization of Int2a, and simply considers that reaction via TS1a generates only CH_3 and its coproduct, because the microcanonical rate constants for reaction via TSa(i) are much larger than the collision frequency and the rate constant for reverse isomerization to regenerate Int1. Thus, condensing the two well system into a one well system, which gives nearly a factor of 4 saving in computational time, has insignificant effects on product yields over the pressures and temperatures modeled.

(iii) Figure 9 shows that the microcanonical rate constants for reaction via TS1b are significantly smaller than those from the competing reaction channels from Int1 at significant energies and may be neglected. Although HCN formation (reaction R4b)

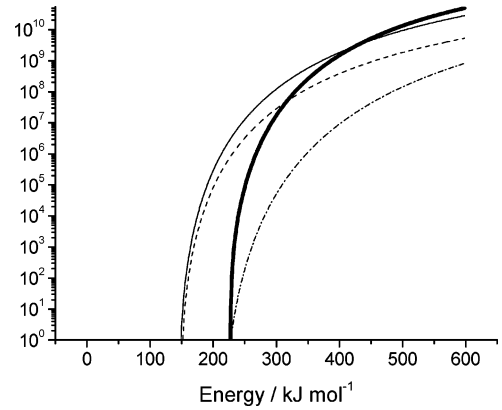

Figure 8. Microcanonical rate constants for channels out of Intl (the secondary radical adduct) where —, $k(E)$ to reactants; — · —, $k(E)$ via TS1b; ---, $k(E)$ via TS1a; and —, $k(E)$ via TS1c.

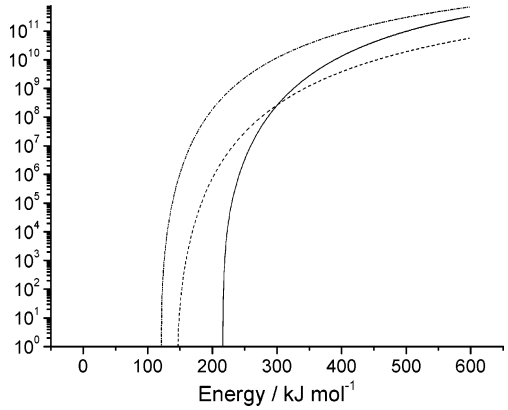

Figure 9. Microcanonical rate constants for channels out of Intal (the primary radical adduct) where where is —, $k(E)$ to reactants; ---, $k(E)$ via TSa2; and — · —, $k(E)$ via TSa1.

is the most thermodynamically favorable channel, it is not a significant channel in this system except possibly via direct abstraction.

(iv) There is no reactive coupling between coupling between Int1 and Inta1, which can be treated using independent MEs. The manner in which each is populated is described by the bimolecular source term included in eq 8.

As noted above, the microcanonical rate constants for dissociation of the initial adducts to regenerate CN, and hence the energy-resolved rates of formation of these adducts, were calculated via an ILT, in which the microcanonical rate constants are linked to $k^{\infty}(T)$ for the association reaction.[36,40,41] The method assumes that the reactants conform to a Boltzmann energy distribution (which is a good approximation at the pressures and timescales of the experiments) and that the reaction follows pseudo-first-order kinetics. Addition of CN to alkenes and alkynes has been shown, by both theory and experiment, to be barrierless,[25,26,30] and CN + propene shows similar behavior, with a weak negative temperature dependence. Thus, the most appropriate form is $k^{\infty}(T) = A(T/300)^n$, which can be equated to the experimentally measured rate coefficient. Reaction via TS1a and TS1c is much faster than either redissociation to regenerate reactants (Figure 8), or collisional stabilization, so that the reaction is at the high pressure limit. Using the data in Table 1 gives the best fit values $A = 3.18 \times 10^{-10}$ cm^3 molecule^{-1} s^{-1} and $n = -0.05$. As discussed below, the relative yields of H and CH_3 obtained from the ME are not sensitive to the values for A and n implemented in the ILT routine.

It remains to determine the relative rates of formation of the initial adducts Int1 and Inta1. A calculation utilizing the ILT technique, assuming that the densities of states and the energies of the two adducts are the sole determinant of the relative rates and hence of the fractionation of the overall rate into the adduct channels, gives 51% of the reaction forming Int1 and the other 49% forming Inta1 over the temperature range of 90−295 K. However, this calculation neglects steric considerations, which we expect will play a role here, with the rate of forming Inta1 (a primary radical) being less than that for Int1 (a secondary radical), because of the interaction between the CN radical and the methyl group in the former case. In the similar reaction of OH + propene, structure activity relations indicate that 87% of the reaction forms the secondary radical adduct and 13% forms the primary radical adduct at 300 K.[42]

In the present case, it was assumed that the canonical rate coefficients, k_{prim} and k_{sec} for formation of Inta1 and Int1, respectively, have the same T dependence, mirroring that of the overall rate coefficient, $k^{\infty}(T)$, so that $A_{Inta1} + A_{Int1} = A = 3.18 \times 10^{-10}$ cm^3 molecule^{-1} s^{-1}. This procedure allows ILT calculations to be performed separately for the two isomers, with the variable parameter, A_{Int1}/A_{Inta1} determined from the fits of the ME to the experimental data.

5.3. Fits to Experimental Data. The ME was used to model the experimental hydrogen yields, α, and to fit the following model parameters: (i) the ratio of the A factors A_{Int1}/A_{Inta1}, (ii) $\langle\Delta E_d\rangle$, and (iii) the energy difference between the threshold energies of TS1a and TS1c, ΔE_{TE}, where

$$\Delta E_{TE} = E(\text{TS1a}) - E(\text{TS1c}) \qquad \text{(E11)}$$

where and E(TS1a) and E(TS1c) are, respectively, the threshold energies of TS1a and TS1c with respect to Int1. For the G3/99 test set of 376 reaction energies, G3X theory has been shown to give a mean absolute deviation from experiment of ∼4 kJ mol^{-1}.[43] Uncertainties in the calculated energies of first-order saddle points are more difficult to quantify, and we adopt this value of 4 kJ mol^{-1} as limits for varying ΔE_{TE}. For the calculations performed herein, ΔE_{TE} was varied about an adjustable mean, E(TS1a) − E(TS1c)/2. The values of $\langle\Delta E_d\rangle$ and A_{Int1}/A_{Inta1} were also left as adjustable parameters. Having defined these four adjustable parameters, an unweighted χ^2 surface over ΔE_{TE} and $\langle\Delta E_d\rangle$ was generated at each value of A_{Inta1}/A_{Int1} and E(TS1a) − E(TS1c)/2 to derive information regarding the combination of parameters that gave the best fits to experimental data. For the CN + propene experimental system at a particular temperature over a range of pressures, P, the following equation was used to define χ^2:

$$\chi^2 = \sum_{P_{exp}} (\alpha_{exp} - \alpha_{ME})^2 \qquad \text{(E12)}$$

where α_{exp} represents the pressure-dependent experimental H atom yield at 298 K and α_{ME} is the predicted pressure-dependent H atom yield at a particular temperature from the ME, as defined in eq E12. In computing the χ^2 fits, 1680 simulations were performed for each of the 12 pressures at which α was measured at 298 K, for a total of 20160 runs. ΔE_{TE} was varied in 1 kJ mol^{-1} steps from −8.0 kJ mol^{-1} ≤ ΔE_{TE} ≤ 5.0 kJ mol^{-1}, $\langle\Delta E_d\rangle$ was varied in 12.5 cm^{-1} steps where 125 cm^{-1} ≤ $\langle\Delta E_d\rangle$ ≤175 cm^{-1}, E(TS1a) − E(TS1c)/2 was varied from 145 to 152 kJ/mol in 0.5 kJ/mol steps, and the ratio of A_{Int1}/A_{Inta1} had values of 70:30%, 80:20%, and 90:10%. Figure 10 shows a plot of χ^2 vs $\langle\Delta E_d\rangle$ and ΔE_{TE} for the values of E(TS1a) − E(TS1c)/2 and A_{Int1}/A_{Inta1}, which give the overall lowest surface minimum. The best fit parameters are as follows: $\langle\Delta E_d\rangle = 145$ cm^{-1}, $\Delta E_{TE} = -5$ kJ/mol, $(\text{TS1a}_{TE} + \text{TS1a}_{TE})/2 = 149$ kJ/mol, and $A_{r,Int1}^{\infty}$:

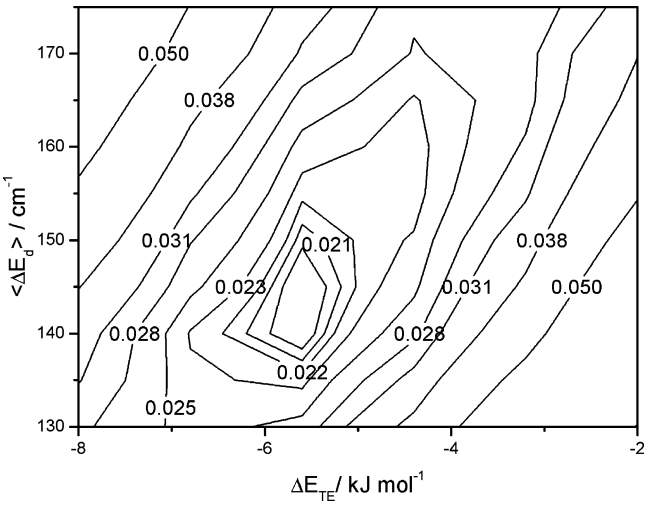

Figure 10. Plot of the best fit 298 K χ^2 surface where $A^{\infty}_{r,\mathrm{Int1}}$: $A^{\infty}_{r,\mathrm{Inta1}}$ is equal to 80:20% and $(\mathrm{TS1a_{TE}} + \mathrm{TS1a_{TE}})/2 = 149$ kJ/mol.

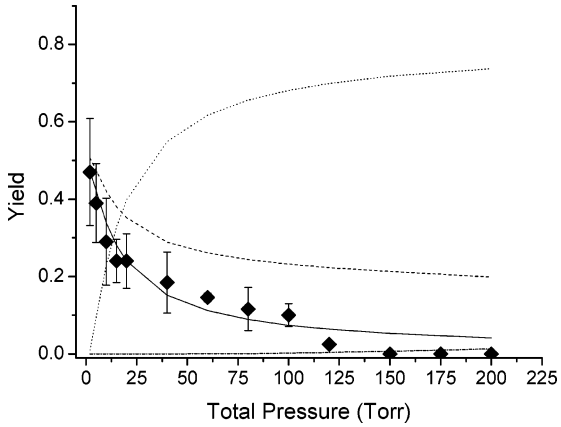

Figure 11. Master equation fit at the χ^2 minimum in Figure 12 as compared with experimentally measured CN + C_3H_6 H atom yields at 298 K over the pressure range 0−200 Torr. The dashed line shows the pressure-dependent CH_3 yields predicted in the ME with the best fit parameter set obtained in Figure 12. Key: ♦, experimental H atom yield; —, ME-fitted H yield; ---, ME-predicted CH_3 yield; ···, ME-predicted Int1 yield; and — · —, ME-predicted Inta1 yield, which is insignificant as compared to the Int1 yield.

$A_{\mathrm{r,Inta1}}^{\infty} = 80{:}20\%$. This ratio of formation of primary and secondary adduct radicals is similar to that derived from structure−activity relations for OH + propene. The value of $(\mathrm{TS1a_{TE}} + \mathrm{TS1a_{TE}})/2$ has only a small impact on the global minimum χ^2, but its value is correlated with the best fit values for $\langle\Delta E_d\rangle$ and ΔE_{TE}, an increase leading to a decrease in the magnitude of ΔE_{TE} and an increase in $\langle\Delta E_d\rangle$. For example, increasing $(\mathrm{TS1a_{TE}} + \mathrm{TS1a_{TE}})/2$ from 148 to 149 kJ/mol gives a χ^2 minimum that is ∼10% worse with an optimum $\langle\Delta E_d\rangle$ of ∼153 $\mathrm{cm^{-1}}$ and a ΔE_{TE} of ∼ −5.5 kJ/mol. The resulting best fit plot from the ME of α vs pressure is shown in Figure 11, together with the yields of CH_3 and of the adducts.

The following conclusions can be drawn from the modeling study and the fits to the experimental data. (i) The zero pressure methyl radical yield is 0.51. Forty percent of this yield derives from formation of the primary addition complex Inta1, and 60% is from 1,2 H atom migration via Int1. Over the pressure range from 0 to 200 Torr, the calculations suggest that of the 20% of CN + propene reacting via Inta1, ∼8% forms Pa1 + H at all pressures, and at 200 Torr, ∼5% is collisionally stabilized. The remainder (92% at 0 pressure and 87% at 200 Torr) goes to P1 + CH_3. Thus, the net pressure-independent H atom yield from this channel is ∼0.016, and the contribution to the net CH_3 yield from this channel varies from 0.184 at zero pressure to 0.174 at 200 Torr.

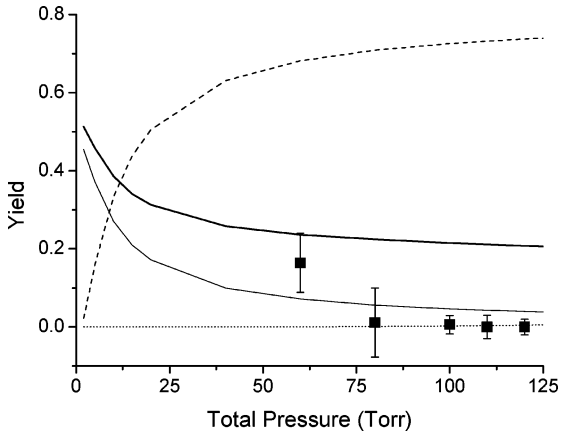

Figure 12. ME-derived radical yields at 195 K. The one-dimensional α^2 best fit attained when $\langle\Delta E_d\rangle = 95.0\ \mathrm{cm^{-1}}$. Key: —, ME H yield; —, ME CH_3 yield; ♦, experimental H yield; ---, ME Int1 yield; and ···, ME Inta1 yield.

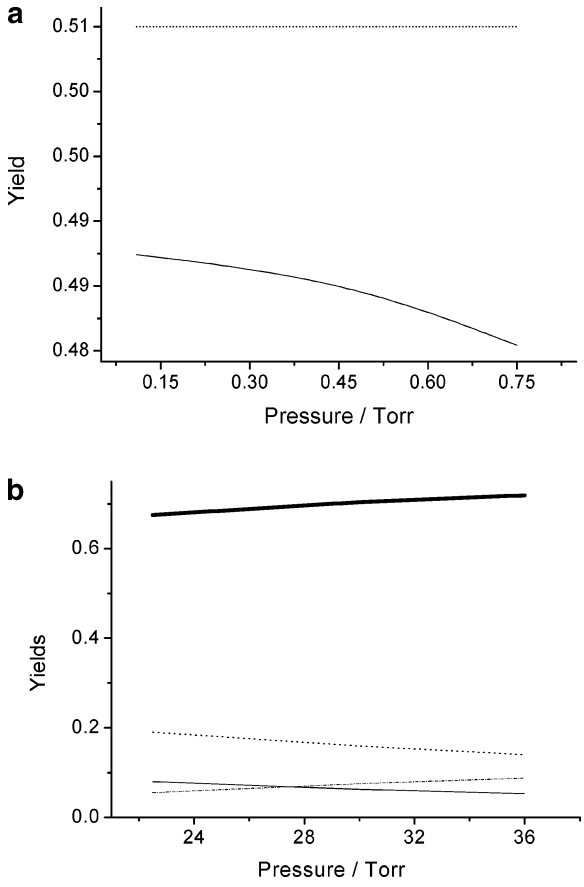

Figure 13. Master equation predictions of H atom yields for conditions on Titan's stratosphere, 160 K (a), and troposphere, 90 K (b). Each plot gives methyl and H yields using a linear model for $\langle\Delta E_d\rangle$ temperature dependence, where $\langle E_d\rangle = 145(T/298)$. Plot a key: ···, ME CH_3 yield; —, ME H yield. The yields of Int1 and Inta1 are trivial. Plot b key: —, ME CH_3 yield; ···, ME CH_3 yield; —, ME H yield; and — · —, ME Inta1 yield.

(ii) Over this pressure range, any reactants that do not go to products are essentially stabilized into Int1, since the amount of Inta1 that is stabilized is trivial. At 200 Torr, no more than 1.5% of the total reactants is stabilized into Inta1.

(iii) The H atom yield is very sensitive to the barrier heights for H atom elimination and H atom migration from the

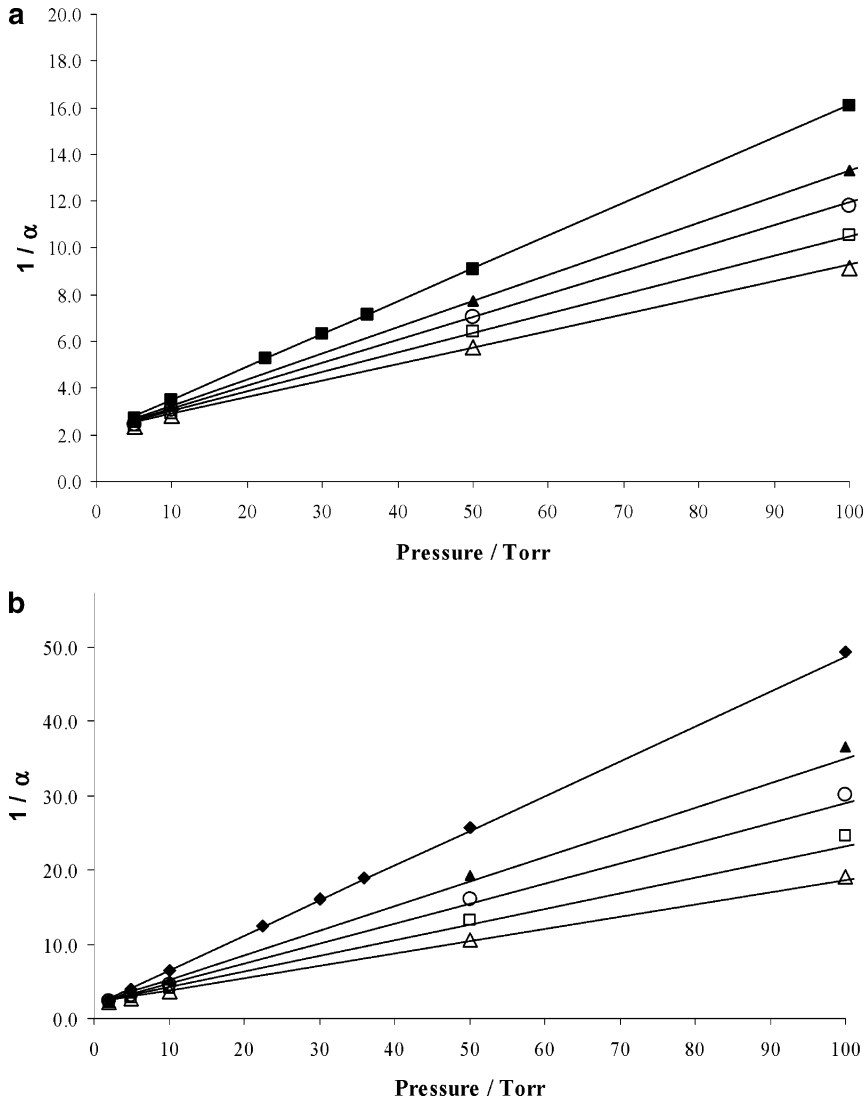

Figure 14. (a) Parametrized ME results for H yields from 1 to 100 Torr and 90−300K. $\langle E_d \rangle = 145(T/298)$, and the data have been fitted with the expression $1/\alpha = [0.737(0.995)^T]P + 1.624(1.001)^T$. Key: ♦, 90 K ME simulations; ▲, 160 K ME simulations; □, 250 K ME simulations; △, 300 K ME simulations; and ○, 200 K ME simulations. (b) Parametrized ME results for CH_3 yields from 5 to 100 Torr and 90−300 K in N_2 bath gas. $\langle E_d \rangle = 145(T/298)$, and the data have been fitted with the expression $1/\alpha = [0.188(0.997)^T]P + 2.067$. Key: ♦, 90 K ME simulations; ▲, 160 K ME simulations; □, 250 K ME simulations; △, 300 K ME simulations; and ○, 200 K ME simulations.

secondary addition complex Int1. Our calculations suggest that the barrier to H atom migration is ∼5 kJ/mol lower than the barrier to H atom elimination. The structure and frequencies for TS1a indicate that H atom migration occurs via a relatively loose transition state, so that this reaction competes effectively with H atom elimination via TS1c except at high energies (see Figure 8).

(iv) The ratio of microcanonical rate coefficients for H and CH_3 elimination from Int2a explains the lack of H production in the CN + *trans*-2-butene reaction (reaction R6). In this reaction, wherever the CN initially adds, there will always be the potential for either CH_3 or H elimination with the former channel being significantly more facile.

(v) The good agreement between experiment and model, which ignores direct abstraction, suggests that abstraction is not occurring to any significant extent. Although our calculations indicate that direct abstraction should be a barrierless process (and hence consistent with the observed negative temperature dependence for k_4), significant direct abstraction would require that more of the complex forming channel leads to H atom production either by more formation of the secondary complex or by a significant change (i.e., outside of the G3X uncertainty limits) in the relative barrier heights for H elimination and H migration out of Int1. The calculations support but cannot confirm the absence of a direct channel; this could be investigated in future experiments as direct abstraction should lead to highly vibrationally excited HCN, which should be readily observable, if occurring.

(vi) The magnitude of $\langle \Delta E_d \rangle$ in this study is comparable to other studies in He bath gas. For example, in a recent ME study on the acetylene + OH system in He bath gas carried out in our lab,[44] the optimum fit to 37 different pressure- and temperature-dependent association rate constants gave a $\langle \Delta E_d \rangle = 149$ cm^{-1} at 298 K, which is very close to the value obtained here of 145 cm^{-1} at 298 K.

5.4. Extrapolation to Conditions Relevant to Titan. The parameters that gave the best fit in Figures 10 and 11 were used to model the experimental data at 195 K. A one-dimensional χ^2 fit was then computed with respect to these data points, varying $\langle \Delta E_d \rangle$ from 37.5 to 150 cm^{-1} in steps of 12.5 cm^{-1}. A $\langle \Delta E_d \rangle$ of ∼100 cm^{-1} gave the best fit to the six pressure-dependent 195 K data points shown in Figure 12. The quality and range of this data set are not as good as those for 298 K because of experimental complications at these lower temper-

TABLE 4: ME Results for CH_3 and H Yields from 0 to 5 Torr and from 90 to 300 K in N_2 Bath Gas with $\langle E_d \rangle = 145(T/298)$

pressure (Torr)	temp (K)	ME H yield	ME CH_3 yield	Int1 yield	Inta1 yield
0.5	90	0.48	0.52	0	0
0.5	160	0.49	0.51	0	0
0.5	200	0.49	0.51	0	0
0.5	250	0.50	0.50	0	0
0.5	300	0.50	0.49	0	0
1.0	90	0.46	0.52	0.022	0
1.0	160	0.47	0.51	0.015	0
1.0	200	0.48	0.51	0.011	0
1.0	250	0.49	0.51	0.010	0
1.0	300	0.49	0.50	0.007	0
2.0	90	0.39	0.47	0.13	0
2.0	160	0.42	0.48	0.10	0
2.0	200	0.44	0.49	0.08	0
2.0	250	0.45	0.49	0.06	0
2.0	300	0.47	0.48	0.05	0
5.0	90	0.25	0.37	0.38	0.0009
5.0	160	0.29	0.39	0.31	0.0008
5.0	200	0.32	0.41	0.27	0.0007
5.0	250	0.35	0.42	0.24	0.0006
5.0	300	0.38	0.43	0.20	0.0006

atures. However, the best fit value allows the temperature dependence of $\langle \Delta E_d \rangle$ to be estimated, facilitating calculation of product yields for the conditions on Titan. A linear dependence of $\langle \Delta E_d \rangle$ on T, $\langle \Delta E_d \rangle = 149(T/298\ \mathrm{K})\ \mathrm{cm}^{-1}$, similar to that obtained in previous work for a He bath gas,[29,45] gives a value of 95 cm^{-1} at 195 K, close to the best fit value of 100 cm^{-1}.

Nitrogen is the dominant gas in the Titan atmosphere, so that $\langle \Delta E_d \rangle$ must be rescaled to account for its higher collisional energy transfer efficiency. The scaling factor was therefore increased from 145 to 250 cm^{-1}, based on recent measurements over this temperature range for OH + C_2H_2.[44] The master equation was then used to model radical yields at the temperatures and pressures on Titan's atmosphere. Figure 13a,b shows ME results for H atom yields at the temperatures and pressures predicted on Titan's troposphere and stratosphere, respectively; the ratio $A_{r,Int1}^{\infty}$:$A_{r,Inta1}^{\infty}$ was maintained at 80:20%. For both of these simulations, there is essentially no pressure stabilization in Inta1 over the pressure ranges investigated so that the remaining product channel is that leading to Int1 by collisional stabilization. In the low pressure regime relevant to Titan's stratosphere, Int1 and Int1a yields are essentially zero.

In addition to the results presented above, the ME was used to model the pressure dependence from 0 to 200 Torr at 90, 160, 250, and 300 K in a nitrogen bath gas. The results are shown in Figure 14a,b. The ME-predicted H yields, α, have been fitted to the expression $1/\alpha = [0.737(0.995)^T]P + 1.624(1.001)^T$, and the CH_3 yields, β, have been fitted to the expression $1/\beta = [0.188(0.997)^T]P + 2.067$. At pressures below ~2 Torr, a linear Stern−Volmer plot does not accurately describe the H yield ME data points, which show curvature that gives yields deviating up to 10% from the linear plots shown. At pressures below ~5 Torr, a linear Stern−Volmer plot does not accurately describe the curvature in the CH_3 yield ME data points, giving CH_3 yields that deviate up to 15% from the linear plot shown. We have not parametrized the ME data in the region of curvature; however, the data for H and CH_3 yields at very low pressures are presented in the Table 4. The ME-predicted Int1 yields, δ, have been fitted to the expression $\delta = 0.8 \times [0.0921(T/300)^{-0.804}P]/(1 + [0.0921(T/300)^{-0.804}P])$ and Inta1 yields, γ, have been fitted to the expression $\gamma = 0.2 \times [0.0131(T/300)^{-0.414}P]/(1 + [0.0131(T/300)^{-0.414}P])$. For the same reasons as for the H and CH_3 yields, the expressions for Int1 and Inta1 were obtained using only data above 5 Torr; the values for the yields at 5 Torr and below are given in Table 4.

6. Conclusions

(i) Rate coefficients have been determined for the first time for CN + *trans*-2-C_4H_8 [$k_{298K} = (2.93 \pm 0.23) \times 10^{-10}$ cm^3 $\mathrm{molecule}^{-1}$ s^{-1}, $k_{195K} = (3.58 \pm 0.43) \times 10^{-10}$ cm^3 $\mathrm{molecule}^{-1}$ s^{-1}] and for CN + *iso*-C_4H_8 [$k_{298K} = (3.17 \pm 0.10) \times 10^{-10}$ cm^3 $\mathrm{molecule}^{-1}$ s^{-1}, $k_{195K} = (4.32 \pm 0.35) \times 10^{-10}$ cm^3 $\mathrm{molecule}^{-1}$ s^{-1}], where the errors represent a combination of statistical uncertainty from the bimolecular plots and an estimate of possible systematic errors based on the standard deviation of repeated determinations at different pressures. Rate coefficients for CN reactions with CH_4, C_2H_2, C_2H_4, and C_3H_6 as measured by CN removal, or where possible H atom growth, are in good agreement with previous work.

(ii) The H atom yields were measured by VUV LIF, calibrating the signals against the unity H atom yield for CN + H_2. The yields at both 298 and 195 K have been shown to be unity within the limits of error for CN + C_2H_2 and C_2H_4, less than 5% for CN + CH_4 and *trans*-2-C_4H_8, and pressure-dependent for CN + C_3H_6 and *iso*-C_4H_8. The intercept on the Stern−Volmer plots (reciprocal yield vs pressure) for the pressure-dependent systems lies at a value greater than one, indicating that there are other active channels for both of these latter reactions.

(iii) To determine the other channel yields, a PES for the CN + propene reaction was calculated and a master equation analysis was performed. The product yields are particularly sensitive to the energy gap between the transition state for the ^{1,2}H shift and that for the H elimination, following addition of CN to form the secondary radical adduct $NCCH_2CHCH_3$; these channels are a common feature in similar systems. Three significant reaction pathways were identified for the CN + propene reaction: (i) direct abstraction of a hydrogen by CN, which appears from the calculations to be a barrierless process; (ii) addition of CN to propene to give the secondary radical; and (iii) addition of CN to propene to give the primary radical, which is ~10 kJ mol^{-1} less stable than the primary radical adduct.

(iv) The best fit parameters from the master equation analysis are an 80% yield for the secondary radical adduct, $\langle \Delta E_d \rangle = 145\mathrm{cm}^{-1}$, and the threshold energies of TS1a and TS1c with respect to Int1 changed from their respective values of 150.0 and 147.1 kJ mol^{-1} to 146.5 and 151.5 kJ mol^{-1}, which is within the G3X uncertainty limits. The direct abstraction channel was not included in the analysis. The quality of the fits suggests that this channel may be insignificant with respect to addition, but it cannot be ruled out.

(v) At 298 K, the H atom yield from the ME analysis is 0.49, in agreement with the value obtained by extrapolation of the Stern−Volmer plot. The ME analysis also provides estimates of the CH_3 yield, which are greater than the H yields at any given temperature and pressure.

(vi) The channel yields were determined using master equation calculations under conditions relevant to Titan's troposphere and stratosphere using the parameter set determined from fits to experimental data at 295 and 195 K, with a scaling of $\langle \Delta E_d \rangle$ to account for the increased rate of stabilization by N_2. H atom and CH_3 production are significant and pressure-dependent, and appropriate parametrizations are given.

(vii) A brute force method has been developed for carrying out very low temperature master equation simulations in an

increased precision environment. It utilizes double−double and quad−double arithmetic.

Acknowledgment. We are grateful to EPSRC for funding through Grant GR/T28560/01 and a studentship for K.L.G. We acknowledge the support of Universities UK and the University of Leeds for an ORS and additional funding for D.G. and thank Prof. Joseph Peeters, Dr. Luc Vereecken, and Dr. Louis Stief for a range of useful discussions. Also, thanks to Dr. David Waller for assistance in implementing the increased precision libraries.

Supporting Information Available: Tables of rovibrational information and energies of the minima and first-order saddle point geometries. This material is available free of charge via the Internet at http://pubs.acs.org.

References and Notes

(1) Chase, M. W. J. *J. Phys. Chem. Ref. Data* **1998**, *9*, 1.
(2) Lebreton, J. P. *Eur. Space Agency Bull.−Space Eur.* **2005**.
(3) Vervack, R. J., Jr.; Sandel, B. R.; Strobel, D. F. *Icarus* **2004**, *170*, 91.
(4) Moses, J. I. *J. Geophys. Res.* **2005**, *110*.
(5) Raulin, F. *Space Sci. Rev.* **2005**, *116*, 471.
(6) Laufer, A. H.; Gardner, E. P.; Kwok, T. L.; Yung, Y. L. *Icarus* **1983**, *56*, 560.
(7) Gupta, S.; Ochiai, E.; Ponnamperuma, C. *Nature (London)* **1981**, *293*, 725.
(8) Lebreton, J. P. *Eur. Space Agency Bull.−Space Eur.* **2004**, 10.
(9) Porco, C. C. *Nature* **2005**, *434*, 159.
(10) Lorenz, R. D.; Dooley, J. M.; West, J. D.; Fujii, M. *Planet. Space Sci.* **2002**, *51*, 113.
(11) Choi, N.; Blitz, M. A.; McKee, K.; Pilling, M. J.; Seakins, P. W. *Chem. Phys. Lett.* **2004**, *384*, 68.
(12) Toublanc, D.; Parisot, J. P.; Brillet, J.; Gautier, D.; Raulin, F.; McKay, C. P. *Icarus* **1995**, *113*, 2.
(13) Haggart, C.; Winkler, C. A. *Can. J. Chem.* **1959**, *37*, 1791.
(14) Haggart, C.; Winkler, C. A. *Can. J. Chem.* **1960**, *38*, 329.
(15) Luque, J.; Crosley, D. R. *SRI Int. Rep.* **1999**, *MP99-009*.
(16) Hilbig, R.; Wallenstein, R. *IEEE J. Quantum Electron.* **1981**, *QE-17*, 1566.
(17) Mahon, R.; McIlrath, T. J.; Myerscough, V. P.; Koopman, D. W. *IEEE J. Quantum Electron.* **1979**, *QE-15*, 444.
(18) Gruebele, M.; Bigwood, R. *Int. Rev. Phys. Chem.* **1998**, *17*, 91.
(19) Sims, I. R. S.; Ian, W. M. *Chem. Phys. Lett.* **1988**, *149*, 565.
(20) Sun, Q. Y. D. L.; Wang, N. S.; Bowman, J. M.; Lin, M. C. *J. Chem. Phys.* **1990**, *93*, 4730.
(21) Blitz, M. A. C. N.; Kovacs, T.; Seakins, P. W.; Pilling, M. J. *Proc. Combust. Inst.* **2005**, *30*, 927.
(22) Pilgrim, J. S.; Taatjes, C. A. *J. Phys. Chem. A* **1997**, *101*, 5776.
(23) Atkinson, R.; Baulch, D. L.; Cox, R. A.; Hampson, R. F., Jr.; Kerr, J. A.; Rossi, M. J.; Troe, J. *J. Phys. Chem. Ref. Data* **2000**, *29*, 167.
(24) Yang, D. L.; Yu, T.; Lin, M. C. *Chem. Phys.* **1993**, *177*, 271.
(25) Balucani, N. *J. Chem. Phys.* **2000**, *113*, 8643.
(26) Vereecken, L.; Groof, D.; Peeters, J. *Phys. Chem. Chem. Phys.* **2003**, *5*, 5070.
(27) Frisch, M. J.; Trucks, G. W.; Schlegel, H. B.; Scuseria, G. E.; Robb, M. A.; Cheeseman, J. R.; Montgomery, J. A., Jr.; Vreven, T.; Kudin, K. N.; Burant, J. C.; Millam, J. M.; Iyengar, S. S.; Tomasi, J.; Barone, V.; Mennucci, B.; Cossi, M.; Scalmani, G.; Rega, N.; Petersson, G. A.; Nakatsuji, H.; Hada, M.; Ehara, M.; Toyota, K.; Fukuda, R.; Hasegawa, J.; Ishida, M.; Nakajima, T.; Honda, Y.; Kitao, O.; Nakai, H.; Klene, M.; Li, X.; Knox, J. E.; Hratchian, H. P.; Cross, J. B.; Bakken, V.; Adamo, C.; Jaramillo, J.; Gomperts, R.; Stratmann, R. E.; Yazyev, O.; Austin, A. J.; Cammi, R.; Pomelli, C.; Ochterski, J. W.; Ayala, P. Y.; Morokuma, K.; Voth, G. A.; Salvador, P.; Dannenberg, J. J.; Zakrzewski, V. G.; Dapprich, S.; Daniels, A. D.; Strain, M. C.; Farkas, O.; Malick, D. K.; Rabuck, A. D.; Raghavachari, K.; Foresman, J. B.; Ortiz, J. V.; Cui, Q.; Baboul, A. G.; Clifford, S.; Cioslowski, J.; Stefanov, B. B.; Liu, G.; Liashenko, A.; Piskorz, P.; Komaromi, I.; Martin, R. L.; Fox, D. J.; Keith, T.; Al-Laham, M. A.; Peng, C. Y.; Nanayakkara, A.; Challacombe, M.; Gill, P. M. W.; Johnson, B.; Chen, W.; Wong, M. W.; Gonzalez, C.; Pople, J. A. *Gaussian 03*, revision B.03; Gaussian, Inc.: Wallingford, CT, 2004.
(28) Klippenstein, S. J.; Miller, J. A. *J. Phys. Chem. A* **2002**, *106*, 9267.
(29) Senosiain, J. P.; Klippenstein, S. J.; Miller, J. A. *J. Phys. Chem. A* **2005**, *109*, 6045.
(30) Balucani, N. A. O.; Huang, L. C. L.; Lee, Y. T.; Kaiser, R. I.; Osamura, Y.; Bettinger, H. F. *Astrophys. J.* **2000**, *545*, 892.
(31) Huang, L. C. L. A. O.; Chang, A. H. H.; Balucani, N.; Lin, S. H.; Lee, Y. T.; Kaiser, R. I. *J. Chem. Phys.* **2000**, *113*, 8656.
(32) Huang, L. C. L. A. O.; Chang, A. H. H.; Balucani, N.; Lin, S. H.; Lee, Y. T.; Kaiser, R. I. *J. Chem. Phys.* **2000**, *113*, 8656.
(33) Sreedhara Rao, V.; Chandra, A. K. *Chem. Phys.* **1995**, *192*, 247.
(34) Blitz, M. A.; Hughes, K. J.; Pilling, M. J. *J. Phys. Chem. A* **2003**, *107*, 1971.
(35) Miller, J. A. K.; Stephen, J. *J. Phys. Chem. A* **2006**, *110*, 10528.
(36) Davies, J. W.; Green, N. J. B.; Pilling, M. J. *Chem. Phys. Lett.* **1986**, *126*, 373.
(37) Frankcombe, T. J.; Smith, S. C. *Comput. Phys. Commun.* **2001**, *141*, 39.
(38) Frankcombe, T. J.; Smith, S. C. *Faraday Discuss.* **2002**, 159.
(39) Hida, Y. L.; Xiaoye S.; Bailey, D. H. *Arithmetic* **2000**, *15*.
(40) Robertson, S. H.; Pilling, M. J.; Baulch, D. L.; Green, N. J. B. *J. Phys. Chem.* **1995**, *99*, 13452.
(41) McKee, K.; Blitz, M. A.; Hughes, K. J.; Pilling, M. J.; Qian, H.-B.; Taylor, A.; Seakins, P. W. *J. Phys. Chem. A* **2003**, *107*, 5710.
(42) Kwok, E. S. C.; Atkinson, R. *Atmos. Environ.* **1995**, *29*, 1685.
(43) Curtiss, L. A.; Redfern, P. C.; Raghavachari, K.; Pople, J. A. *J. Chem. Phys.* **2001**, *114*, 108.
(44) McKee, K. W. B.; Mark A.; Cleary, P. A.; Glowacki, D. R.; Pilling, M. J.; Seakins, P. W.; Wang, L. *J. Phys. Chem. A* **2007**, *111*, 4043.
(45) Blitz, M. A.; Hughes, K. J.; Pilling, M. J.; Robertson, S. H. *J. Phys. Chem. A* **2006**, *110*, 2996.
(46) Sims, I. R. Q. J.-L.; Travers, D.; Rowe, B. R.; Herbert, L. B.; Karthauser, J.; Smith, I. W. M. *Chem. Phys. Lett.* **1993**, *211*, 461.
(47) Yang, D. L.; Yu, T.; Wang, N. S.; Lin, M. C. *Chem. Phys.* **1992**, *160*, 317.
(48) Herbert, L.; Smith, I. W. M.; Spencer-Smith, R. D. *Int. J. Chem. Kinet.* **1992**, *24*, 791.
(49) Lichtin, D. A.; Lin, M. C. *J. Chem. Phys.* **1986**, *104*, 325.
(50) Lichtin, D. A.; Lin, M. C. *J. Chem. Phys.* **1985**, *96*, 473.
(51) Schacke, H.; Wagner, H. G.; Wolfrum, J. *Ber. Bunsenges. Phys. Chem.* **1977**, *81*.
(52) North, S. W.; Fei, R.; Sears, T. J.; Hall, G. E. *Int. J. Chem. Kinet.* **1997**, *29*, 127.
(53) Butterfield, M. T.; Yu, T.; Lin, M. C. *Chem. Phys.* **1993**, *169*, 129.